Chinese Chemical Letters 35 (2024) 109199

Contents lists available at ScienceDirect

Chinese Chemical Letters

journal homepage: www.elsevier.com/locate/cclet

Synergistic enhancement of chemotherapy for bladder cancer by photothermal dual-sensitive nanosystem with gold nanoparticles and PNIPAM

Xiangqian Cao[a,1], Chenkai Yang[a,1], Xiaodong Zhu[b,1], Mengxin Zhao[b], Yilin Yan[a], Zhengnan Huang[a], Jinming Cai[a], Jingming Zhuang[a], Shengzhou Li[a], Wei Li[b,*], Bing Shen[a,*]

[a] Department of Urology, Shanghai General Hospital, Shanghai Jiao Tong University School of Medicine, Shanghai 200080, China
[b] Department of Nanomedicine & Shanghai Key Lab of Cell Engineering, Naval Medical University, Shanghai 200433, China

ARTICLE INFO

Article history:
Received 2 July 2023
Revised 10 October 2023
Accepted 12 October 2023
Available online 13 October 2023

Keywords:
Doxorubicin
Gold nanoparticles
Thermosensitive polymer
Photothermal therapy
Bladder cancer

ABSTRACT

Bladder cancer is a common malignant tumor of the urinary system with the potential to be treated by nano drug delivery system. The current work describes the synthesis and characterization of a novel nanomaterial to construct a nano-carrier based on 1-palmitoyl-2-oleoyl-*sn*-glycerol-3-phosphatecholine (POPC) loaded doxorubicin (DOX) and embedded with gold nanoparticles and poly(*N*-isopropyl acrylamide) (PNIPAM) (GNPS@PNIPAM-POPC-DOX, GPPD). The dual-sensitive nanosystem gives simultaneous photothermal treatment and chemotherapy for bladder cancer. *In vitro* and *in vivo* properties were assessed using bladder cancer cell lines and mice and GPPD system distribution, tumor inhibition, and biocompatibility are reported. The system had favorable stability, low biological toxicity, controlled release efficiency, photothermal synergistic action, efficient photothermal transition, and favorable tumor suppressive effects. As a result, GPPD is a potential therapeutic approach for bladder cancer.

Bladder cancer is the 9th most prevalent cancer type and ranks fourth globally among diseases affecting males [1,2]. Conventional chemotherapy drugs, particularly doxorubicin (DOX), may be effective but targeting is poor, and significant side effects occur, including impaired bone marrow hematopoietic function and cardiotoxicity. Nanotechnology may improve drug accumulation and targeting of bladder cancer cells by increasing the efficiency of drug delivery. Thus, novel nanomedicine treatments are urgently required to facilitate chemotherapy [3,4].

Delivering drugs to the tumor region is a challenge in cancer therapy. Lipid-based organelles, such as liposomes, which are spherical vesicles with a phospholipid bilayer may be used to encapsulate chemotherapeutic agents and show promise for drug delivery [5]. Liposomes have low toxicity and good biocompatibility and prevent drug leakage in the circulation, controlling drug release at tumor areas and increasing intratumor concentration. Enhanced permeability and retention (EPR) effects of solid tumor tissues damages microvessels and lymphatic vessels and aids the accumulation of liposomes or macromolecules in tumors [6]. Drug resistance and bladder cancer progression limit the therapeutic effect of conventional chemotherapy and off-target drug distribution leads to adverse reactions and low intratumor drug accumulation. Encouragingly, liposomes may overcome some of these difficulties and aid chemotherapeutic drug delivery [7].

Advanced photothermal materials, such as gold nanoparticles (GNPs), have indicated the potential of photothermal therapy (PTT) [8–10]. GNPs are laser-activated photothermal therapeutic agents [11] and their physicochemical, optical, and electronic properties make them suitable for biomedical applications [12–14]. The small and spherical nanoparticles produce fluorescent/thermal/reactive oxygen species under near-infrared (NIR) light. Adriamycin-loaded GNPs have been shown to have slower drug release and prolonged systemic circulation compared with free adriamycin-loaded PLZ4-nanoporphyrin (PNP) [15], showing them to be multipurpose agents for thermal ablation and drug delivery [16]. Intravenous injection of NIR radiation-absorbing gold-silicon nano shells resulted in the clearance of the majority from the blood and retention in the bladder for 30–50 min, where particles were distributed throughout the bladder wall in the tumor-associated stroma [17,18]. PTT under NIR light excitation thus has considerable specificity [19]. Poly(*N*-isopropyl acrylamide) (PNIPAM) is a

* Corresponding authors.
E-mail addresses: liwei_dds@163.com (W. Li), urodrshenbing@shsmu.edu.cn (B. Shen).
[1] These authors contributed equally to this work.

https://doi.org/10.1016/j.cclet.2023.109199
1001-8417/

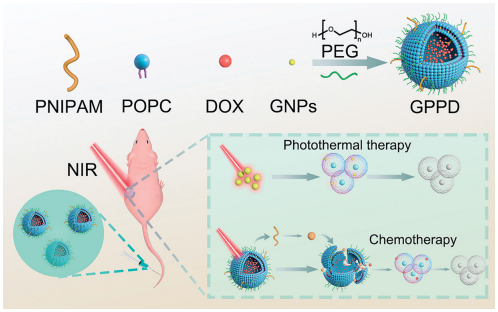

Fig. 1. The system model was assembled using a rotary steam bottle, and the protective shell was made of PEG. The system was embedded with GNPs and PNIPAM to form a functional GPPD structure for delivering chemotherapy drugs. The figure is a schematic diagram of the mechanism of killing tumor cells by GPPD in mice. GPPD was injected into mice through the tail vein, and GNPs exerted photothermal therapeutic effects under NIR light and disintegration of the system enabled the synergistic release of chemotherapeutic agents to kill tumor cells.

novel temperature-sensitive polymer and is used for the integration of photothermal transition particles, including GNPs [20–22]. The resulting nanoparticles allow the enhancement of liposome-delivered intratumor drugs and have the potential to reduce side effects.

However, chemotherapeutic drugs have been widely used clinically for various cancers. Chemotherapy is not effective, Shi *et al.* found that pH-sensitive nanomaterials for anti-tumor drug delivery are stronger than chemotherapy alone [23]. Li *et al.* found that synergistic effects of chemotherapy and PTT applied to nanomaterials produced favorable therapeutic effects [24]. Therefore, combining chemotherapy and PTT for synergistic treatment of bladder cancer is highly promising.

Liposomes containing DOX and embedded with GNPs and PNIPAM to form a functional GPPD structure were constructed during the current study. After NIR light irradiated the cells in the tumor region, the gold nanoparticles locally generated heat and produced a photothermal therapeutic effect, which killed the tumor cells. In addition, contraction denaturation of the PNIPAM structure led to structural disintegration, releasing gold nanoparticles and chemotherapeutic agents, further facilitating PTT and chemotherapy (Fig. 1). GPPD was injected into mice through the tail vein and accumulation in tumor regions and tumor apoptosis promoted under 808 nm NIR light irradiation. High cytotoxicity was produced from the photothermal conversion of the GNPs with NIR light irradiation. Thermal stimulation caused PNIPAM to undergo a coil-like to spherical transition which ruptured the liposomes, allowing DOX to be released [25]. The GNPs embedded in the liposomes enhanced the PNIPAM phase transition by increasing the local temperature when excited by NIR light. As a result, GNPs and DOX had a synergistic effect on bladder cancer.

1-Palmitoyl-2-oleoyl-*sn*-glycerol-3-phosphatecholine (POPC) was used for liposome construction [26] and GNPs and PNIPAM dendritic molecules were embedded in the membrane. GNPs were adsorbed onto polymers modified with polyethylene glycol (PEG) and PNIPAM by positive and negative charges for liposome insertion (Table S1 in Supporting information). The physical and chemical properties of GPPD were adjusted during self-assembly by fine-tuning the composition of GNPs, POPC, PEG, and PNIPAM to form nanoparticles with a defined structure.

The PNIPAM low critical solution temperature (LCST) was approximately 32 °C but could be modified and that of GPPD was approximately 42 °C (Fig. 2A). GNP- and DOX-loaded polymers thus had temperature-controlled release. GNP and GPPD size distributions were evaluated by dynamic light scattering (DLS). The particle size increased after GNPs embedding on the liposome membrane with a size of 400–500 nm. The particle size of GPPD was also increased after irradiation by NIR light (Table S1). GPPD doped with PNIPAM showed an increase in particle size after NIR irradiation and became spherical due to self-polymerization (Fig. 2B). Good photothermal conversion *in vitro* was shown (Figs. 2A and B). The photothermal conversion efficiency (η) of GPPD was 16.3% (Fig. S1 in Supporting information). GPPD had a volume phase transition temperature of approximately 42 °C. POPC delivery of DOX and NIR irradiation of GNP, which led to the breakage of hydrogen bonds as the temperature increased, gave the system reduced toxicity. PNIPAM underwent a chain to globular shape transition, enlarging the liposome void and releasing the drug. The photothermal PNIPAM contraction, which allowed controlled drug release, indicated successful system construction and precipitated tumor cell death. PNIPAM contraction produced thermosensitive changes which mediated passive targeting [27]. Therapeutic nanomedicine applications of the photothermal properties of gold have previously been demonstrated by Zhang *et al.* [28]. The combination of GNP and PNIPAM has great potential to improve past research results. Transmission electron microscopy (TEM) was used to examine the GNPs (Fig. 2C) and the size of the GPPD was found to be approximately 400–500 nm (Fig. 2D). A similar value was derived by DLS. The DLS (Table S1) and TEM (Figs. 2C and D) data demonstrated the successful synthesis of the system. The photothermal

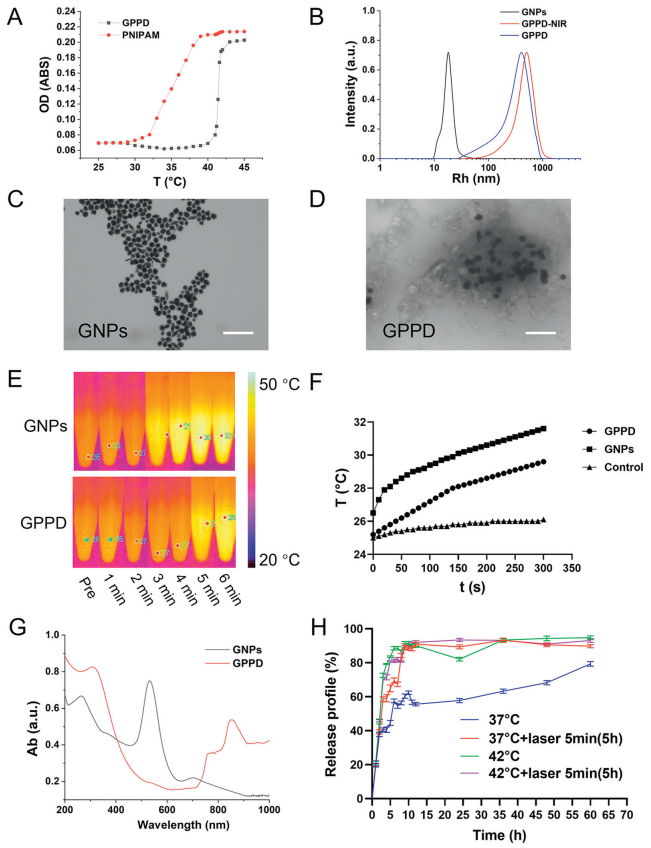

Fig. 2. (A) Discriminant volume phase transition temperature (VPTT) by UV–vis spectrophotometer determination of optical density (OD) value, testing the same concentration of PNIPAM in anhydrous ethanol solution and the temperature dependence of the GPPD radius. (B) Particle size distribution of GNPs, GPPD, and GPPD-NIR. (C, D) TEM images of GNPs and GPPD system (scale bar: 100 nm). (E) Photothermal images of GNPs and GPPD were captured using an infrared camera. (F) Photothermal effect of GPPD, GNPs and the control group (ddH_2O) *in vitro*. (G) DLS. Light absorption curve of GNPs (100 μg/mL) and GPPD (100 μg/mL). (H) Release curve of *in vitro* GPPD at 37 and 42 °C and GPPD at 37 and 42 °C with a laser (808 nm), $n = 3$. Data are mean ± standard deviation (SD).

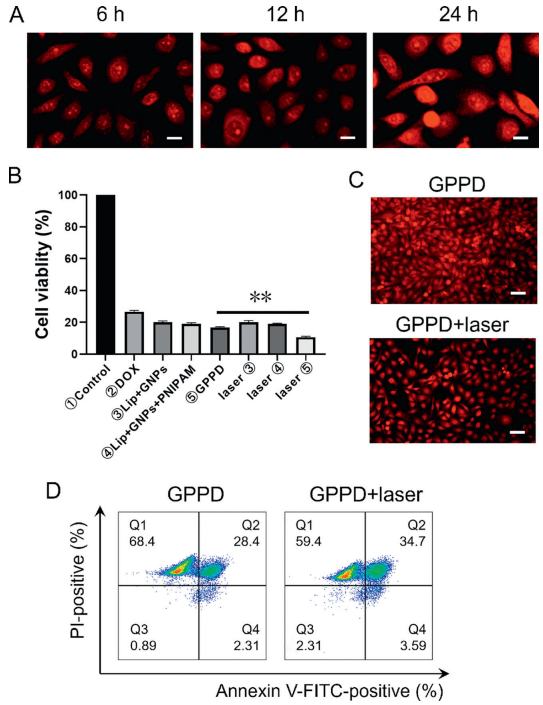

Fig. 3. (A) 5637 cells absorb assessment GPPD at 6, 12, and 24 h (scale bar: 10 μm). (B) CCK-8 assay of 5637 cells. (C) 5637 cells condition of GPPD and GPPD with laser. After 5 min laser irradiation for GPPD, 5637 cells continued to develop 24 h (scale bar: 100 μm). (D) Scatter plots of apoptosis in 5637 cells measured by flow cytometry for GPPD and GPPD with laser, $n = 3$. Data are mean ± SD. $^{**}P < 0.01$.

conduction efficiency of 100 μg/mL GNPs and GPPD with continuous NIR light (808 nm, 1 W/cm^2, 6 min) at different time points allowed the temperature to increase with illumination duration (Fig. 2E). The favorable photothermal conversion efficiency would facilitate the PNIPAM structural transformation which enables drug release. The photothermal effect of 100 μg/mL GNP was greater than that of 100 μg/mL GPPD and both were good relative to ddH_2O (Fig. 2F). Small GNPs were readily embedded into the liposome membrane for tissue permeability and retention. The GPPD encapsulation efficiency was 48.21% and drug loading was 17.84% (Table S1). The percentage of GNPs and PNIPAM in GPPD nanoparticles analyzed by thermal gravimetric analyzer (TGA) was 9.37% and 26.58% (Fig. S2 in Supporting information). Ultraviolet–visible spectroscopy (UV–vis) measured GNP absorbance at 400–600 nm and GPPD at 800–1000 nm (Fig. 2G). The 808 nm laser was chosen for subsequent experiments. Drug release was stimulated by laser irradiation for 5 min at 37 °C and also by increased temperature so that the drug could be measured in the solution (Fig. 2H). However, liposomes failed to reach a stable drug release plateau quickly at 37 °C *in vitro*. Laser irradiation caused the tumor microenvironment to achieve a temperature that exceeded the GPPD LCST of 42 °C with the result that PNIPAM released the chemotherapeutic drugs. In summary, GPPD with temperature-controlled release and photothermal synergy was successfully constructed.

Inverted fluorescence microscopy was used to observe the endocytosis of GPPD, 5637 human bladder cancer cells were treated with 10 mg/mL GPPD. Subsequently, dead cells were washed away with PBS, and drug accumulation was observed from 6 h to 24 h in the nucleus (Fig. 3A). GNPs interacted with organelles and lysosomes induced apoptosis [29,30]. The nuclear binding of DOX is shown in Fig. 3A. Cell counting kit-8 (CCK-8) assays showed the half maximal inhibitory concentration (IC_{50}) to be 10.8 mg/mL (GPPD) and 2.5 mg/mL (DOX) for bladder cancer cells and these concentrations were used with a 2 h incubation for subsequent experiments (Fig. S3 in Supporting information). Laser irradiation enhanced cytotoxicity, reducing the number of bladder cancer cells, and GPPD produced higher cytotoxicity than GNPs. The photothermal effect was monitored with an inverted fluorescence microscope after NIR light exposure (Figs. 3B and C). The combination index (CI) value is 0.22 according to the cell viability measured by single DOX and combined drugs, which indicated a strong synergistic effect of GPPD (Fig. S3). Flow cytometry showed that irradiation increased apoptosis in bladder cancer cells (Fig. 3D). Cancer cell apoptosis has been reported to be driven by mitochondrial signals [31,32].

Animal welfare and experimental procedures were reviewed and approved by the Animal Ethics Committee of Shanghai General Hospital (No. 2021KY046). Photothermal effects of GPPD and GNPs were tested *in vivo* and intratumor injection gave a weaker effect of GPPD than of GNPs (Fig. 4A). Tail vein administration of GPPD to tumor-bearing mice followed by NIR light irradiation showed the highest tumor volume for GPPD with laser treatment, followed by DOX and GPPD (Figs. 4B and C). No change was seen for mouse body weight (Fig. 4D). Tumor inhibition rates (TIR) were 34.7% for GPPD, 52.9% for DOX, and 91.2% for GPPD with the laser treatment (Fig. 4E). Mice were injected and irradiated on 0, 2 and 4 d and sacrificed on 14 d (Fig. 4F) for harvesting of tumors (Fig. 4G) and hematoxylin-eosin (HE) staining (Fig. 4H). The photothermal effect and tumor suppression were higher for GPPD with laser than for GPPD alone, perhaps due to the EPR effect. Thus, GPPD with laser treatment appeared to promote bladder cancer cell death.

GPPD was stable (Fig. S4 in Supporting information) with no sedimentation or variation in particle size (Table S2 in Supporting information), and biocompatibility tests, involving injection of 200 μL GPPD (4 mg/kg) every two days for a total of 3 times, in ICR mice showed no significant effect of the drugs on mouse survival. The mice were in good condition with no significant abnormalities after one month. HE staining of the liver, heart, spleen, lung and kidney indicated favorable GPPD biocompatibility (Fig. S5 in Supporting information). Therefore, GPPD appeared to be suitable for human use.

Administration of fluorescein isothiocyanate (FITC)-loaded but DOX-free liposomes to tumor-bearing mice showed insignificant tumor site enrichment of FITC but significant enrichment was observed after laser irradiation. Accumulation was seen in the liver, heart, and lung after 2 h but minimal tissue content after 24 h, indicating good biocompatibility (Figs. S6A–J in Supporting information). Drug release and accumulation were promoted by the use of the laser after both 2 and 24 h, demonstrating the passive targeting property of GPPD (Figs. S6K–N in Supporting information). Temperature-responsive structures have previously been shown to improve cellular uptake and drug release [33]. Although the current drug system had a good targeting capacity, its tissue retention capacity requires further improvement. Targeting and retention were improved by increasing the administration frequency but this represents a shortcoming of the system. Nonetheless, NIR light improved GPPD enrichment in tumor tissues.

In conclusion, a thermo- and chemotherapy-sensitive dual-function GPPD liposome structure was constructed. The EPR effect of GPPD, with stable mosaic structure and excellent biocompatibility, led to accumulation at tumor sites. Drugs were released into the tumor region by the PNIPAM-regulated photothermal effect of GNPs, leading to the accumulation of high concentrations of DOX. Co-therapy with NIR light-induced chemotherapy and PTT has an anti-tumor effect *in vivo* and *in vitro*. Moreover, GPPD has the advantage over the previous tissue ablation strategies since normal tissue is preserved. We introduce the NIR light-dependent nanodrug delivery system of GPPD with therapeutic potential for drug delivery in bladder cancer.

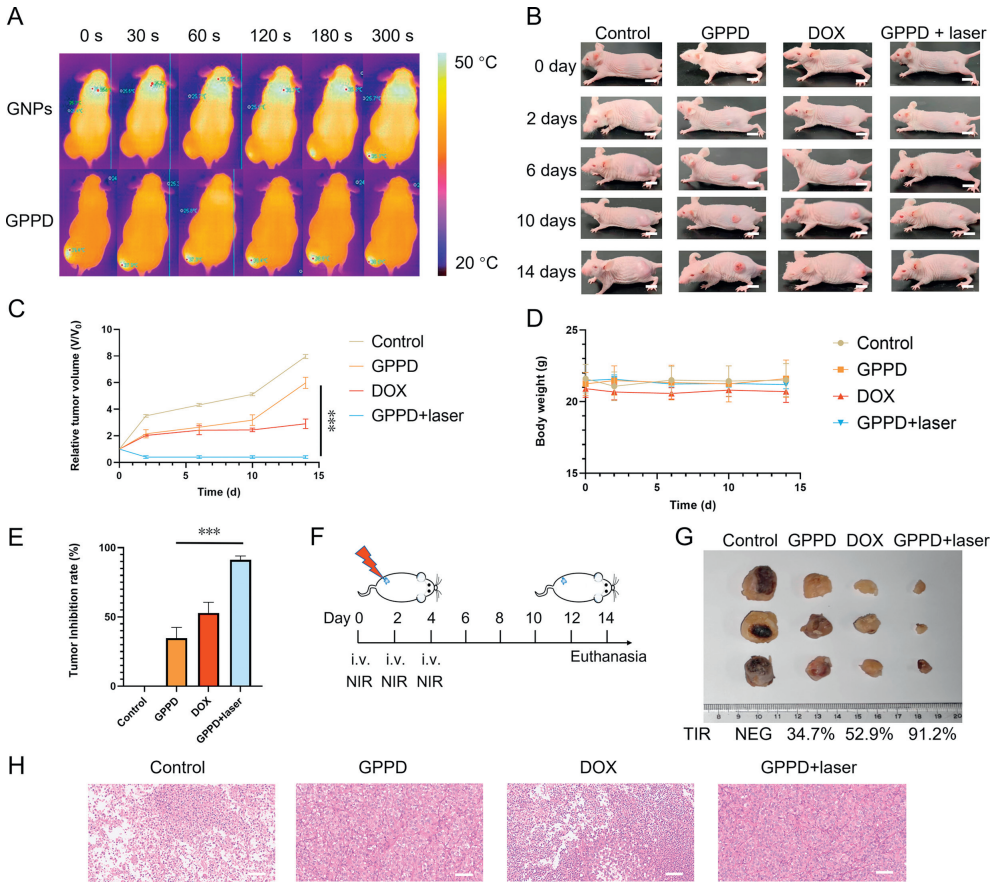

Fig. 4. There were four groups in the anti-tumor effect experiment: the PBS group, DOX group, GPPD group, and GPPD with NIR light irradiation group. (A) The photothermal effect of 808 nm excitation light in tumor-bearing mice was observed by an infrared camera. (B) A tumor suppression test was performed in the control group, GPPD group, DOX group, and GPPD group with laser, and tumor growth was observed (0, 2, 6, 10 and 14 d) (scale bar: 5 cm). (C) Changes in relative tumor volume (V/V_0) in each group, $n = 3$. (D) Body weight changes in each group, $n = 3$. (E) Tumor inhibition rates of different groups were calculated, $n = 3$. (F) The experimental schedule *in vivo*, from 0 d to 14 d. (G) The collected tumors in the different group treatments with the measurement scale. (H) HE staining results of tumors (scale bar: 100 μm). Data are mean ± SD. $^{***}P < 0.001$.

Declaration of competing interest

The authors declare that they have no known competing financial interests or personal relationships that could have appeared to influence the work reported in this paper.

Acknowledgments

This work was funded by the National Natural Science Foundation of China (Nos. 92059112, 82072821 and 31470964), the Shanghai Songjiang Municipal Science and Technology Commission Natural Science Foundation (No. 20SJKJGG250), University of Shanghai for Science and Technology (No. 10–21–302–405) and sponsored by the Program of Shanghai Academic Research Leader (No. 22XD1404700). EditSprings provided the linguistic services.

Supplementary materials

Supplementary material associated with this article can be found, in the online version, at doi:10.1016/j.cclet.2023.109199.

References

[1] T. Tate, T. Xiang, S.E. Wobker, et al., Nat. Commun. 12 (2021) 6160.
[2] R.L. Siegel, K.D. Miller, N.S. Wagle, et al., CA Cancer J. Clin. 73 (2023) 17–48.
[3] P. Jain, H. Kathuria, M. Momin, Pharmacol. Ther. 226 (2021) 107871.
[4] J. Gao, S. Ma, X. Zhao, et al., Chin. Chem. Lett. 32 (2021) 3954–3961.
[5] Q. Xiao, X. Li, C. Liu, et al., Chin. Chem. Lett. 33 (2022) 4191–4196.
[6] S.K. Huang, E. Mayhew, S. Gilani, et al., Cancer Res. 52 (1992) 6774–6781.
[7] N. Wang, Y. Zuo, S. Wu, et al., Acta Pharm. Sin. B 12 (2022) 4486–4500.
[8] C. Huang, L. Zhang, Q. Guo, et al., Adv. Funct. Mater. 31 (2021) 2010637.
[9] Q. Li, Z. Shi, F. Zhang, et al., Acta Pharm. Sin. B 12 (2022) 107–134.
[10] C. Lin, H. Hao, L. Mei, et al., Smart Mater. Med. 1 (2020) 150–167.
[11] X. Li, J.F. Lovell, J. Yoon, et al., Nat. Rev. Clin. Oncol. 17 (2020) 657–674.
[12] M.H. Jazayeri, T. Aghaie, R. Nedaeinia, et al., Cancer Immunol. Immunother. 69 (2020) 1833–1840.
[13] S.K. Cho, K. Emoto, L.J. Su, et al., J. Biomed. Nanotechnol. 10 (2014) 1267–1276.
[14] T. Chen, W. Zeng, C. Tie, et al., Bioact. Mater. 10 (2022) 515–525.
[15] T.Y. Lin, Y. Li, Q. Liu, et al., Biomaterials 104 (2016) 339–351.
[16] L.R. Hirsch, R.J. Stafford, J.A. Bankson, et al., Proc. Natl. Acad. Sci. U. S. A. 100 (2003) 13549–13554.
[17] D.P. O'Neal, L.R. Hirsch, N.J. Halas, et al., Cancer Lett. 209 (2004) 171–176.
[18] H.M. Smilowitz, L.J. Tarmu, M.M. Sanders, et al., Int. J. Nanomedicine 12 (2017) 7937–7946.
[19] J.K. Cheong, V. Popov, E. Alchera, et al., Comput. Biol. Med. 138 (2021) 104881.
[20] Y. Kwon, Y. Choi, J. Jang, et al., Pharmaceutics 12 (2020) 204.
[21] R. Yadav, S. Kumar, P. Narang, et al., J. Colloid Interface Sci. 582 (2021) 478–487.
[22] H. Wang, X. Yang, C. Hu, et al., Chin. Chem. Lett. 33 (2022) 4179–4184.
[23] Z. Shi, Q. Li, L. Mei, Chin. Chem. Lett. 31 (2020) 1345–1356.
[24] Z. Li, Y. Yang, H. Wei, et al., J. Control. Release 338 (2021) 719–730.
[25] W. Li, M. Nakayama, J. Akimoto, et al., Polymer 52 (2011) 3783–3790.
[26] D. Petroni, C. Riccardi, D. Cavasso, et al., Molecules 26 (2021) 6591.
[27] X. Zhu, Y. Sun, D. Chen, et al., J. Control. Release 254 (2017) 107–118.
[28] H. Zhang, J. Lu, Y. Zhang, et al., Chin. Chem. Lett. 34 (2023) 107450.
[29] F. Zhang, Y. Hou, M. Zhu, et al., Adv. Sci. 8 (2021) e2102666.
[30] F. Zhang, D. Chen, Y. Wang, et al., Nanomedicine 12 (2017) 1575–1589.
[31] F. Zhang, X. Zhu, J. Gong, et al., Nanomedicine 11 (2016) 1993–2006.
[32] M. Yu, J. Yu, Y. Yi, et al., J. Control. Release 347 (2022) 104–114.
[33] W. Li, J. Li, J. Gao, et al., Biomaterials 32 (2011) 3832–3844.